

Matching creeping waves with lit area diffraction field

Anna Kirpichnikova

Division of Computing Science and Mathematics, University of Stirling, UK;
e-mail: anya@cs.stir.ac.uk

Natalia Kirpichnikova

St. Petersburg Department of Steklov's Mathematical Institute; e-mail: nkirp@pdmi.ras.ru

We continue explorations of the shortwave plane wave diffraction for an axisymmetric elongated body. The previously obtained formulae for the boundary currents were evaluated numerically and showed matching in the borders of the regions going from the lit zone into the shadow. The results are presented for the case of both Dirichlet and Neumann boundary conditions.

1 INTRODUCTION

This paper gives an update on the ongoing project with previous results published in [3] - [8]. We consider a three-dimensional body of revolution Ω (called a scatterer). The body is axisymmetric, strictly convex, and prolate. Assume the surface $\partial\Omega$ of the scatterer is generated by revolving in $\varphi \in [0, 2\pi]$ a plane convex curve $x = \gamma(z)$ around the z -axis, i.e.,

$$x = \gamma(z) \cos \varphi, \quad y = \gamma(z) \sin \varphi,$$

in a Cartesian coordinate system x, y, z , see Figure 1.

A cross-section of $\partial\Omega$ by a plane $z = 0$ is called an Equator and it coincides with the shadow-light boundary created by the plane incident wave $U^{\text{inc}} = \exp(ikz)$, $k = \frac{2\pi}{\lambda} \gg 1$ which radiates along the axis of revolution z . Here λ is a wavelength.

The five zones of our interest (see Figure 1) are correspondingly, Zone 1 is an illuminated region, Zone 2 is a neighbourhood of the limit ray touching point (called the Fock's region), Zone 3 is a penumbra region, Zone 4 is a shadow region, Zone 5 is a surface shadow layer.

1.1 Problem formulation

We introduce an orthogonal geodesic field formed by parallels and meridians that follow the shape of $\partial\Omega$. We denote by n the distance along the outward normal \mathbf{n} . We denote by s the arc length (distance) along the meridians counted from the Equator. The

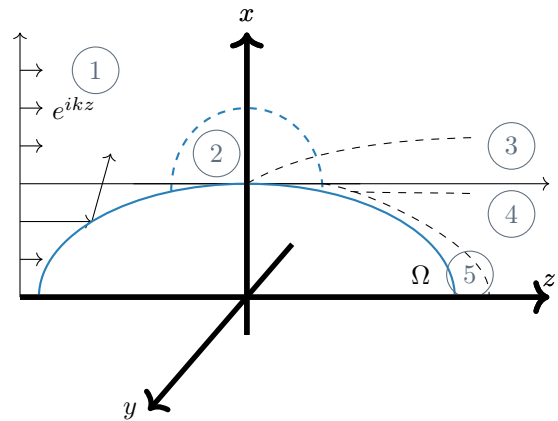


Figure (1) Five different zones around the scatterer.

curvature of a meridian at a point $s \in \partial\Omega$ is denoted by $\frac{1}{\rho(s)}$.

We consider Helmholtz equation with either Dirichlet or Neumann boundary conditions on $\partial\Omega$

$$(\Delta + k^2)U = 0, \quad \frac{\partial}{\partial n}U|_{n=0} = 0 \text{ or } U|_{n=0} = 0, \quad (1)$$

with decay at infinity conditions, namely, $U \rightarrow 0$ as $r \rightarrow \infty$.

1.2 Main method

We use the Fock-Leontovich parabolic equation method [1] in a vicinity of some point of $\partial\Omega$ that belongs to the border of geometric shadow region, together with several classical methods from [2], [9], [10], and [11].

We use the following expansion of the total field $U = e^{iks}W$, and the first three terms of the asymptotic expansion

$$W = W_0 + \frac{W_1}{k^{\frac{1}{3}}} + \frac{W_2}{k^{\frac{2}{3}}} + \dots, \quad k \gg 1. \quad (2)$$

These terms in the expansion satisfy a recurrent

system of differential equations

$$\begin{aligned} \mathcal{L}_0 W_0 &= 0, \quad \mathcal{L}_0 W_1 + \mathcal{L}_1 W_0 = 0, \\ \mathcal{L}_0 W_2 + \mathcal{L}_1 W_1 + \mathcal{L}_2 W_0 &= 0, \dots \end{aligned} \quad (3)$$

We keep an eye on two large parameters in the expansion. One is the Fock's large parameter

$$\mathbf{M}_0 = \left(\frac{k\rho_0}{2} \right)^{\frac{1}{3}},$$

the second one is a parameter of body prolongation

$$\mathbf{\Lambda}_0 = \frac{\rho_0}{\gamma(0)}.$$

Here $\rho_0 = \rho(0)$ is the geodesic meridians curvature radius at the light-shadow boundary (the Equator) where $s = 0$. At the same time, the radius of curvature of the geodesics (meridians) and the transversal radius of curvature of the Equator are assumed to satisfy the inequalities

$$k\rho(0) \gg 1, \quad k\gamma(0) \gg 1, \quad \text{as } k \rightarrow \infty.$$

In the Fock's region (2), we introduce stretched coordinates (σ, ν) instead of (s, n) in the following way:

$$\begin{aligned} \sigma &= \frac{k^{1/3}s}{2^{1/3}\rho_0^{2/3}} = \frac{\mathbf{M}_0 s}{\rho_0}, \\ \nu &= \frac{2^{1/3}k^{2/3}n}{\rho_0^{1/3}} = \frac{2n\mathbf{M}_0^2}{\rho_0}. \end{aligned} \quad (4)$$

The prolonged shape of the scatterer reveals itself in the second large parameter $\mathbf{\Lambda}_0$, which is the ratio of longitudinal and transversal curvature radii. Parameter $\mathbf{\Lambda}_0$ only appears in W_2 of the expansion (2).

We assume the total field satisfies the following expansion

$$U = e^{iks} \left[\sum_{j=0}^2 \frac{W_j}{k^{j/3}} + \mathcal{O}(k^{-1}) \right], \quad W_j = W_j^{\text{inc}} + W_j^{\text{ref}}.$$

1.2.1 Plane wave diffraction: Incident field

The asymptotic expansion terms for the field W_i^{inc} , $i = 0, 1, 2$, take the form of the contour integrals of the linear combination of Airy functions $v(t)$ and their derivatives $v'(t)$, and polynomials of integration variable and a dimensionless coordinate ν of order $2j$ at $v(t)$, and of order $2j - 1$ at $v'(t)$ in

zone (2). The integration contour Γ goes along the straight line from $\infty e^{i\frac{2\pi}{3}}$ to 0, and then from 0 to ∞ along the positive real axis in the complex plane of ζ .

1.2.2 Plane wave diffraction: Reflection

As for W_j^{ref} , $j = 0, 1, 2$, one should replace Airy functions $v(t), v'(t)$ with $w_1(t), w_1'(t)$, then their form would be similar to the ones of W_j^{inc} . Functions $w_1(t), w_1'(t)$ satisfy the limiting absorption principle as $\nu \rightarrow +\infty$.

Besides, W_j^{ref} also satisfy the following recurrent system of differential equations similar to system (3).

1.2.3 Fock's famous formulae

The main terms of the asymptotic expansion (denoted by subscript 0 in this paper) of the total wave field can be constructed in the neighbourhood of the $s = 0$ point, in zone (2)

$$U_0^{\text{Dir}} = e^{iks} (W_0^{\text{inc}} + W_0^{\text{ref}}) =$$

$$\frac{e^{iks}}{\sqrt{\pi}} \int_{\Gamma} e^{i\sigma\zeta} \left[v(\zeta - \nu) - \frac{v(\zeta)}{w_1(\zeta)} w_1(\zeta - \nu) \right] d\zeta, \quad (5)$$

$$U_0^{\text{Neu}} = \frac{e^{iks}}{\sqrt{\pi}} \int_{\Gamma} e^{i\sigma\zeta} \left[v(\zeta - \nu) - \frac{v'(\zeta)}{w_1'(\zeta)} w_1(\zeta - \nu) \right] d\zeta. \quad (6)$$

The integration contour Γ can be taken the same as in Subsection 1.2.1.

1.2.4 Shadow zones

Now we consider shadow zones, see Figure 2. The arclength in zone (5) $s = \mathcal{O}(1)$, and the normal $\nu(s, n)$ is defined by

$$\nu(s, n) = \frac{k^{\frac{2}{3}} n 2^{\frac{1}{3}}}{\rho^{\frac{1}{3}}(s)}, \quad \nu(s, n) = \mathcal{O}(1). \quad (7)$$

Hence, the Fock's large parameter $\mathbf{M}_0(s)$ depends on s in zone (5). Taking into account the residues, we get the following main term representations

$$U_{0K}^{\text{Dir}} = e^{iks} (-2\sqrt{\pi}i) \sum_{p=1}^K e^{i\sigma\zeta_p} \frac{w_1(\zeta_p - \nu)}{[w_1'(\zeta_p)]^2} \quad (8)$$

and

$$U_{0K}^{\text{Neu}} = e^{iks} (2\sqrt{\pi}i) \sum_{p=1}^K e^{i\sigma\zeta_p'} \frac{w_1(\zeta_p' - \nu)}{[w_1(\zeta_p')]^2}, \quad (9)$$

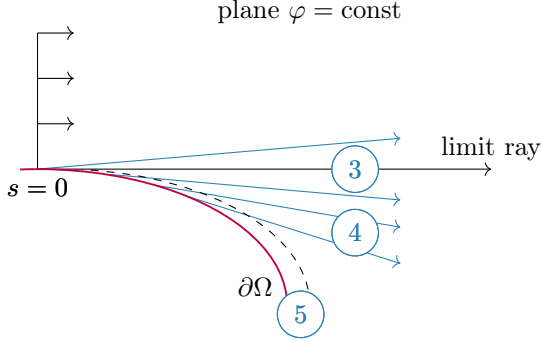


Figure (2) Penumbra and shadow regions. The field in the shadow region (4) between regions (3) and (5) has ray nature of the leaving wave. Region (5) is the creeping waves zone with $\nu = \mathcal{O}(1)$, $s = \mathcal{O}(1)$.

in zone (5) for the Dirichlet and Neumann boundary conditions correspondingly. Here $w_1(\zeta_p) = 0$ and $w_1'(\zeta_p) = 0$, and K counts the number of the roots taken into account.

2 NUMERICAL MATCHING IN THE LIT ZONES

Zone (5) in local coordinates (σ, ν) corresponds to the conditions $\sigma \rightarrow +\infty$ and $\nu = \mathcal{O}(1)$.

First of all, we made sure the following functions match their classical definitions (see [1])

$$f(\sigma) = \frac{1}{\sqrt{\pi}} \left[\int_{\Gamma} \frac{e^{i\sigma\zeta}}{w_1(\zeta)} d\zeta \right]; \quad F(\sigma) = e^{i\sigma^3/3} f(\sigma),$$

$$g(\sigma) = \frac{1}{\sqrt{\pi}} \left[\int_{\Gamma} \frac{e^{i\sigma\zeta}}{w_1'(\zeta)} d\zeta \right]; \quad G(\sigma) = e^{i\sigma^3/3} g(\sigma),$$

and their asymptotics are as follows

$$\text{Im}(F) \rightarrow 2\sigma, \quad \text{Re}(G) \rightarrow 2, \quad \text{as } \sigma \rightarrow -\infty.$$

The dimensionless Dirichlet current, obtained in [3], has the form

$$k^{-1} I_0^{\text{Dir}} = \frac{1}{M_0 \sqrt{\pi}} \left[\int_{\Gamma} \frac{e^{i\sigma\zeta}}{w_1(\zeta)} d\zeta + \frac{\Lambda_0}{2M_0^2} \int_{\Gamma} e^{i\sigma\zeta} \left[\frac{\zeta}{w_1(\zeta)} - \frac{[w_1'(\zeta)]^2}{[w_1(\zeta)]^3} \right] d\zeta \right]. \quad (10)$$

It was compared to its main approximation

$$k^{-1} I_0^{\text{Dir}} \approx \frac{1}{M_0} e^{-i\frac{\sigma^3}{3}} F(\sigma) = \frac{1}{M_0} f(\sigma)$$

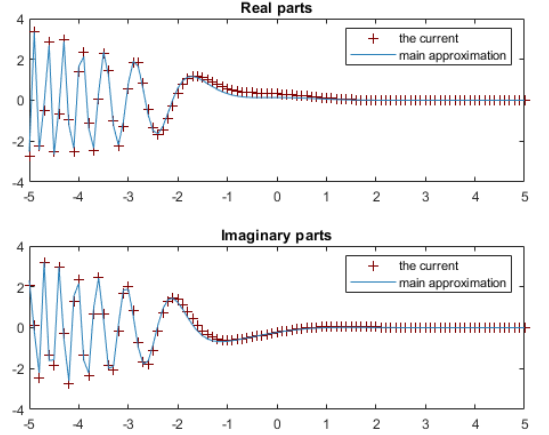


Figure (3) Matching the dimensionless Dirichlet current with the main term for $-5 < \sigma < 5$.

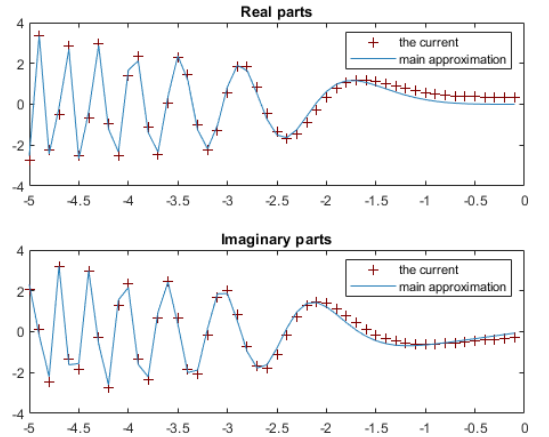


Figure (4) Matching the dimensionless Dirichlet current with its asymptotics as $\sigma \rightarrow -\infty$ for $k\rho = 50$.

for $k\rho(0) = 20$ and $k\rho(0) = 50$, see Figure (3) for the illustration of the case $k\rho(0) = 50$. The picture for $k\rho(0) = 20$ is pretty similar and hence omitted here. The choice of the numerical values for the simulations is justified in [6]. The current (10) was also compared to the asymptotics of its main approximation

$$k^{-1} I_0^{\text{Dir}} \approx 2i\sigma \left(\frac{1}{M_0} \right) e^{-i\frac{\sigma^3}{3}}$$

as $\sigma \rightarrow -\infty$ for $k\rho(0) = 20$ and $k\rho(0) = 50$, following [5], see Figure 4. The dimensionless Neumann

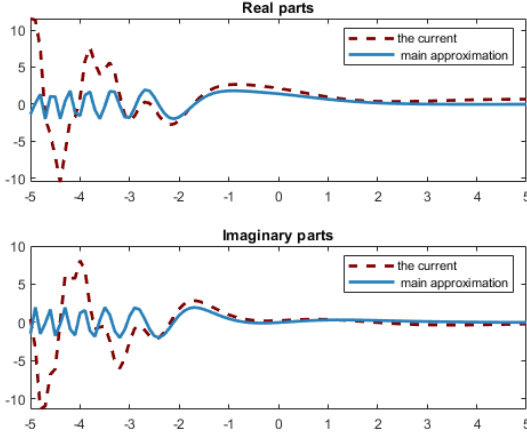


Figure (5) Matching the dimensionless Neumann current with its main approximation for $k\rho = 50$.

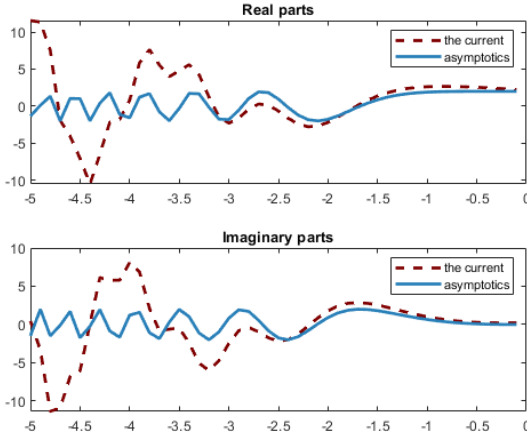


Figure (6) Matching the dimensionless Neumann current with its asymptotics at $\sigma \rightarrow -\infty$ for $k\rho = 50$.

current, obtained in [4], has the following form

$$k^{-1}I^{\text{Neu}} = \frac{1}{\sqrt{\pi}} \left[\int_{\Gamma} \frac{e^{i\sigma\zeta}}{w_1'(\zeta)} d\zeta + \frac{1}{M_0^\varepsilon} \int_{\Gamma} e^{i\sigma\zeta} \left[\frac{\zeta}{w_1'(\zeta)} - \frac{\zeta^2 w_1^2(\zeta)}{[w_1'(\zeta)]^3} \right] d\zeta \right]. \quad (11)$$

It was first compared to its main approximation $I_0^{\text{Neu}} \approx g(\sigma)$, see Figure 5 and then compared to the asymptotics of its main approximation $I_0^{\text{Neu}} \approx 2e^{-i\frac{\sigma^3}{3}}$ when $\sigma \rightarrow -\infty$, see Figure 6.

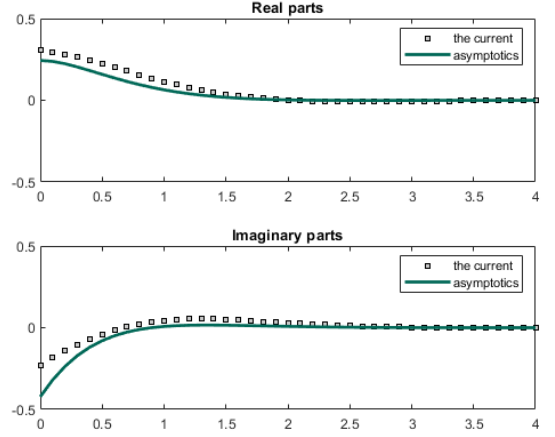


Figure (7) Comparison of the Dirichlet currents with its asymptotics for $\sigma > 0$.

The difference between the Dirichlet (10) and Neumann currents (11) is in the order of their amplitudes: the amplitude of $k^{-1}I^{\text{Dir}}$ is of order $\mathcal{O}(M_0^{-1})$ compared with the amplitude of $k^{-1}I^{\text{Neu}}$.

3 NUMERICAL JUSTIFICATION OF THE TRANSITION TO THE SHADOW ZONE

The incident field does not penetrate into the shadow zone (5), but it remains in the boundary layer $\nu = \mathcal{O}(1)$, and with $s > 0$ increasing, the observation point (s, ν) appears to be in (5). It is convenient to lift the integration contour up into the upper half-plane (where $\text{Im}(\zeta) > 0$, $\sigma \rightarrow +\infty$), as the exponent $e^{i\sigma\zeta}$ decays as fast as $\exp(-\sigma \text{Im} \zeta)$. This will lead to keeping only a few roots ($w_1(\zeta_p) = 0$ for Dirichlet and $w_1'(\zeta_p) = 0$ for Neumann) in the expansion.

Since the slowest decay of the exponents of (8), (9) is due to the first root $\zeta_1(\zeta_1')$, we will further consider only ζ_1, ζ_1' instead of the sum in the above formulae (8), (9), and will work with U_{01} , namely, see formulae (8), (9) for $K = 1$.

Shadow zone asymptotics for the F and G functions when $\sigma > 0$ are

$$F(\sigma) \approx e^{i\left(\frac{\sigma^3}{3} + \frac{\sigma|\zeta_1|}{2}\right)} c_1 e^{-\sigma|\zeta_1| \frac{\sqrt{3}}{2}},$$

$$c_1 = 1.8325, \zeta_1 = 2.22811 \cdot e^{i\frac{\pi}{3}}, \sigma > 0,$$

$$G(\sigma) \approx e^{i\left(\frac{\sigma^3}{3} + \frac{\sigma|\zeta_1'|}{2}\right)} c_2 e^{-\sigma|\zeta_1'| \frac{\sqrt{3}}{2}},$$

$$c_2 = 1.8325, \zeta_1' = 1.01879 \cdot e^{i\frac{\pi}{3}}, \sigma > 0.$$

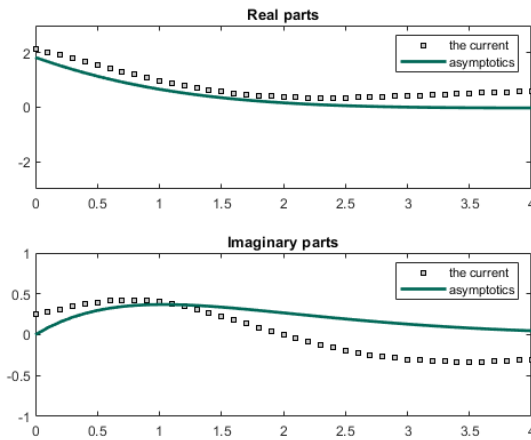


Figure (8) Comparison of the Neumann current with its asymptotics for $\sigma > 0$.

3.1 Matching currents when going into the shadow

We match Dirichlet current (10) with the following shadow asymptotics for large positive σ (see Figure 7)

$$k^{-1}I_0^{\text{Dir}} \approx \frac{1}{M_0} \frac{2\sqrt{\pi}i}{w_1'(\zeta_1)} e^{\frac{\sigma|\zeta_1|}{2}(i-\sqrt{3})}$$

to reveal pretty good match.

Similar match was found for the Neumann current (11) when we compare it to the following shadow asymptotics

$$k^{-1}I_0^{\text{Neu}} \approx \frac{2\sqrt{\pi}i}{\zeta_1' w_1(\zeta_1')} e^{\frac{\sigma|\zeta_1|}{2}(i-\sqrt{3})}$$

for positive σ , see Figure 8.

4 CONCLUSION

The following results were obtained in the project so far. The representation of the wave field in the Fock's zone with the first three terms of the expansion was obtained in [3] for the Dirichlet case, and in [4] for the Neumann case. Also the influence of the prolongation parameter has been established. The wave field currents were obtained and compared numerically with their the asymptotic expansions. The main terms of the expansions were compared with their asymptotics also. The obtained expressions were used as initial conditions for the field in the shadow zone, where the solution takes form of a sum of the residues in the roots of the denominator of the integrand.

It is interesting what happens if we go away from the boundary. If the observation point $M(s, \nu)$ goes out of the surface layer ($n \sim \mathcal{O}(k^{-\frac{2}{3}})$), then $\nu \gg 1$ and Airy function w_1 can be replaced with its asymptotics as $\nu \rightarrow +\infty$. Going away from the scatterer, the ray field of creeping waves corresponds to the behaviour of leaving wave which has the scatterer as a caustic (at least in the main approximation). It would be interesting to consider what happens away from the scatterer numerically. Also it is interesting to visualize the creeping wave in the shadow zone.

ACKNOWLEDGEMENTS

The work was partially supported by the RFBR grant No. 20-01-0067. The authors are very grateful to the anonymous reviewers for their valuable comments.

REFERENCES

- [1] V.A. Fock, Electromagnetic Diffraction and Propagation Problems, International Series of Monographs on Electromagnetic Waves, vol. 1, Pergamon Press (1965).
- [2] V.M. Babich, V. Buldyrev, Asymptotic Methods in Short-Wavelength Diffraction Theory, Alpha Science, Oxford (2007).
- [3] N.Ya. Kirpichnikova, M.M. Popov, *The Leontovich-Fock parabolic equation method in problems of short-wave diffraction by prolate bodies*. Journal of MSci, **194**, No.42, (2013), 30–43.
- [4] N.Ya. Kirpichnikova, A.S. Kirpichnikova, *Leontovich-Fock Parabolic Equation Method in the Neumann Diffraction Problem on a Prolate Body of Revolution*. Journal of MSci, **238**, No.5, (2019), 658–675.
- [5] M.M. Popov, N.M. Semtchenok, N.Ya. Kirpichnikova, *On short-wave diffraction by strongly prolate body of revolution* — J. Mathem.Sciences **226**, No. 6 (2017), 795–809.
- [6] M.M. Popov, N.M. Semtchenok, N.Ya. Kirpichnikova, *On Short-Wave Diffraction by an Elongated Body. Numerical Experiments*. — J. Mathem.Sciences **226**, No. 6 (2017), 734–743.

- [7] A. Kirpichnikova, N. Kirpichnikova, *Comparison of the currents in the Dirichlet and Neumann shortwave diffraction problems of a plane wave from smooth prolate bodies of revolution*. Proceedings of IEEE 2018 Days on Diffraction conference (2018), 161–167.
- [8] N.Ya. Kirpichnikova, A.S. Kirpichnikova *Creeping waves in the shadow region with the Dirichlet and Neumann conditions*. 2019 Days on Diffraction (DD), St. Petersburg, Russia, 2019, pp. 89-93, doi: 10.1109/DD46733.2019.9016422.
- [9] V.M. Babich, N.Ya. Kirpichnikova, *The Boundary-Layer Method in Diffraction Problems*, Springer-Verlag (1979).
- [10] Friedlander F.G., Keller J.B. *Asymptotic expansion of solution of $(\nabla^2 + k^2)u = 0$* . Comm. Pure Appl. Math, **8**, No. 3, (1955), 378–394.
- [11] Keller J.B., *Diffraction by a convex cylinder*. Trans. IRE Ant. and Prop., **4**, No. 3, (1956), 312–321.